Chinese Chemical Letters 34 (2023) 108229

Contents lists available at ScienceDirect

Chinese Chemical Letters

journal homepage: www.elsevier.com/locate/cclet

Dissolved oxygen in aeration-driven piezo-catalytic for antibiotics pollutants removal in water

Minxian Zhang[b], Wanqian Guo[a,*], Yingyin Chen[b], Dechun He[c,*], Abdulgalim B. Isaev[d], Mingshan Zhu[a,b,*]

[a] State Key Laboratory of Urban Water Resource and Environment, Harbin Institute of Technology, Harbin 150090, China
[b] School of Environment, Jinan University, Guangzhou 510632, China
[c] Research Team of Soil and Rural Eco-environment, South China Institute of Environmental Sciences, MEE, Guangzhou 510655, China
[d] Department of Inorganic Chemistry and Chemical Ecology, Dagestan State University, M. Gadjieva 43a, Makhachkala 367001, Russian Federation

ARTICLE INFO

Article history:
Received 22 November 2022
Revised 9 February 2023
Accepted 13 February 2023
Available online 17 February 2023

Keywords:
Aeration
Piezo-catalysis
Dissolved oxygen
Reactive oxygen species
Antibiotic removal

ABSTRACT

The misuse of antibiotics and oxygen-lacking in aquaculture causes serious water environmental problems. Herein, a piezoelectic odd-layered MoS_2 is prepared and applied to piezo-catalytic remove tinidazole (TNZ) and other antibiotic pollutants with aeration as a piezo-driving force. About 89.6% of TNZ can be degraded by MoS_2 under aeration in the presence of dissolved oxygen with a reaction rate constant of 0.15 min^{-1}, which is 2.4 times higher than that under N_2 atmosphere and quiescence conditions. Quenching experiments and electron paramagnetic resonance (EPR) tests identify that singlet oxygen ($^1O_2$) and superoxide radical ($O_2^{\bullet-}$) are dominant reactive oxygen species in MoS_2/aeration system. These results demonstrate that MoS_2 can trigger a piezoelectric effect and produce charge carriers to generate reactive oxygen species with dissolved oxygen (DO) for contaminant degradation with the turbulence and water bubbles rupture driven by aeration.

The rapid development of aquaculture is caused by the increased demand for seafood [1,2]. In high-density aquaculture plants, antibiotics are extensively used to deal with bacterial infections and increase seafood production. However, a large portion of antibiotics cannot be absorbed by aquaculture organisms and released into aquaculture water, leading to the accumulation by degrees in the aquatic environment, thereby posing a potential threat to the ecological environment and human health [3–6]. Biological treatment technology is the conventional approach employed to dispose aquaculture wastewater owing to its low cost and energy consumption, but it cannot degrade antibiotics effectively [7–9]. Therefore, developing effective processes are important to degrade antibiotics from aquaculture wastewater.

Piezoelectricity, as a kind of typical physical phenomenon, is mediated by a transformation of mechanical energy to polarized charges, which has been broadly applied in wastewater treatment [10–17]. However, most reported studies achieved a piezoelectric effect from ultrasonic vibration with a relatively high frequency (kHz), leading to high energy consumption to restrict the potential application. Therefore, it is urgent to capture a low-frequency force for piezoelectric effect motivation. Recently, Zhu's group novelty constructed a self-powered reactor to simulate pipeline drainage for organic pollutants removal [18,19] and disinfection [20]. Ao *et al.* also studied the important role of hydrodynamic factors in piezo-photocatalytic process with ZnO nanorod array [21]. In the field of aquaculture, aeration is always used to improve the content of dissolved oxygen (DO), thereby prolonging the lifetime of aquaculture organisms [22,23]. Such an aeration process provides a possibility to induce piezoelectric effect by means of turbulence and water bubbles rupture. It is also worth studying the contribution of DO offered by aeration for reactive oxygen species (ROS) generation in piezo-catalytic degradation reactions.

In this work, an aeration device was introduced to simulate the aeration process in aquaculture, which triggered the piezoelectric effect to degrade antibiotic tinidazole (TNZ) using an odd-layered MoS_2. TNZ is one of the typical and most frequently detected antibiotics in aquatic environment, which is hardly decomposed *via* conventional wastewater treatment technologies due to its high bioaccumulation potential and low biodegradability [24,25]. The results showed that MoS_2 exhibits a higher removal efficiency of TNZ under aeration of DO than that under N_2 atmosphere and quiescent conditions. The intrinsic mechanisms of the piezo-catalytic

* Corresponding authors.
E-mail addresses: guowanqian@hit.edu.cn (W. Guo), hedechun@scies.org (D. He), zhumingshan@jnu.edu.cn (M. Zhu).

https://doi.org/10.1016/j.cclet.2023.108229
1001-8417/

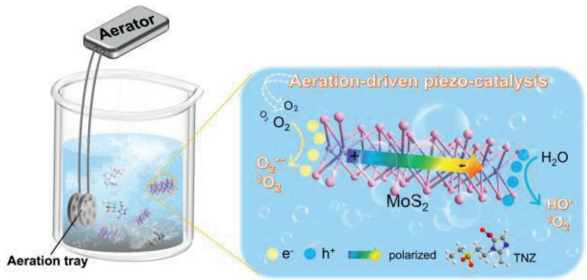

Fig. 1. Schematic diagram of piezo-catalytic TNZ degradation using MoS_2 under aeration.

degradation were revealed by scavenger experiments and electron paramagnetic resonance analysis. Moreover, a liquid chromatography quadrupole time-of-light tandem mass spectrometry (LC-TOF-MS) was further used to identify the degradation intermediates and pathways of TNZ degradation. The turbulence and water bubbles driven by aeration worked as the piezoelectric force to trigger piezo-catalysis, and also provided sufficient DO to generate ROS for the decomposition of organic contaminants. The strategy based on piezo-catalysis using MoS_2 under aeration to solve aquaculture water pollution is described as Fig. 1.

All reagents, preparation, and characterization of MoS_2, along with analysis methods are shown in Text S1 (Supporting information). As shown in Figs. S1-S3 (Supporting information), the as-synthesized MoS_2 was characterized by X-ray diffraction (XRD), transmission electron microscope (TEM), and X-ray photoelectron spectroscopy (XPS). As depicted in Fig. S1, the peaks at 13.8°, 32.4°, and 57.4° can be indexed to (002), (100), and (110) crystal planes of MoS_2 (JCPDS No. 37–1492) [26], respectively, demonstrating a successful preparation of MoS_2. The TEM image of MoS_2 in Figs. S2a and b exhibits an odd-layers structure of MoS_2, in which the lattice spacing of 0.63 nm is ascribed to the (002) crystallographic plane [27]. The XPS spectra in Fig. S3a present that there are two peaks at 228.2 eV and 231.3 eV assigned to Mo $3d_{5/2}$ and Mo $3d_{3/2}$ (Fig. S3b in Supporting information) [28,29], while S $2p_{3/2}$ and S $2p_{1/2}$ are located at 161.1 eV and 162.4 eV (Fig. S3b) [30]. Besides, the piezoelectric property of as-prepared MoS_2 is verified by piezoelectric force microscope (PFM), piezoelectric current density, and electrochemical impedance spectroscopy (EIS). From Fig. S4 (Supporting information), MoS_2 showed a polarized rotation of 180° in the phase-voltage loop and the amplitude-voltage loop exhibited a typical butterfly-shape curve, suggesting an excellent piezoelectric polarization of MoS_2 [31]. Fig. S5a (Supporting information) presents that MoS_2 exhibited a prompt piezoelectric current response during consecutive on-off aeration cycles, while a semicircular Nyquist diagram of the MoS_2 was smaller than that obtained under static conditions, suggesting a smaller resistance (Fig. S5b in Supporting information) [32]. All proofs above set a solid foundation for a well-synthesized MoS_2 with strong piezoelectric response.

The water bubbles rupture driven by aerator in Fig. S6 (Supporting information) was employed as the piezo-driving force to study the influence of turbulence driven by aeration and DO in MoS_2/aeration system, control experiments included MoS_2 (Quiescent), MoS_2/aeration, and MoS_2/N_2 system were compared. As depicted in Fig. 2a, the removal rate of TNZ was achieved at 89.6% in the MoS_2/aeration system, while it decreased to 59.9% in the MoS_2/N_2 system. In contrast to MoS_2 (Quiescence) system (2.1% removal rate of TNZ), the degradation activity of MoS_2/N_2 system may due to the water bubbles rupture generated by aeration resulting in a piezoelectric polarization of MoS_2 to produce polarized carriers such as electron (e^-) and hole (h^+) to directly remove TNZ. Moreover, the first-order kinetics model of TNZ degradation was employed and shown in Fig. 2b. The reaction rate constant k of the MoS_2/aeration system ($k = 0.15\ min^{-1}$) is 2.4 times higher than the sum of MoS_2/N_2 system ($k = 0.061\ min^{-1}$) and MoS_2 (Quiescent) system ($k = 0.0014\ min^{-1}$), revealing the significant roles in the co-presence of aeration and DO for TNZ degradation.

To ascertain the ROS of TNZ degradation with MoS_2, quenching experiments were performed by using isopropanol (IPA), *p*-benzoquinone (*p*-BQ), L-histidine (L-His), potassium dichromate ($K_2Cr_2O_7$), and potassium iodide (KI) as scavengers [33,34]. Fig. 2c shows that the degradation rate of TNZ was not obviously suppressed with the addition of IPA (decreased to 79.2%), while a 66.1% removal rate was achieved in the presence of $K_2Cr_2O_7$, which indicated a minor contribution of $HO^{\bullet}$ and e^- on TNZ degradation. Besides, the introduction of *p*-BQ, KI, and L-His restrained the efficiency to 38.3%, 45.4%, and 49.1%, confirming that $O_2^{\bullet-}$, h^+, and $^1O_2$ played dramatic roles in TNZ degradation. For a deep understanding, electron paramagnetic resonance (EPR) tests were used to identify the generation of ROS in the piezo-catalytic process. As depicted in Figs. 2d-f, the signals of DMPO-$HO^{\bullet}$, DMPO-$O_2^{\bullet-}$, and TEMP-$^1O_2$ were detected in the MoS_2/aeration process, while no

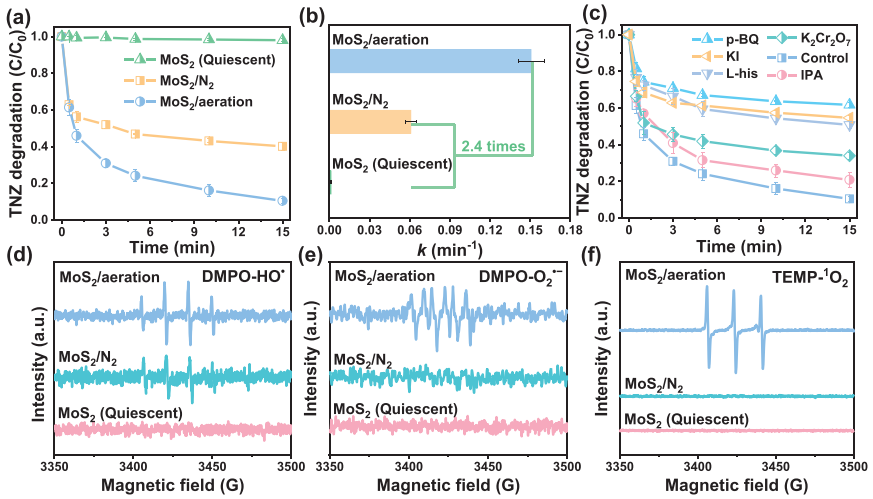

Fig. 2. (a) Degradation efficiencies and (b) *pseudo*-first-order kinetics of TNZ degradation under various oxidation systems. (c) Quenching experiments in MoS_2/aeration system for TNZ degradation. EPR spectra for the detection of (d) $HO^{\bullet}$, (e) $O_2^{\bullet-}$, and (f) $^1O_2$ under different catalytic systems. Experimental conditions: [TNZ] = 10 mg/L, [MoS_2] = 0.5 g/L, aeration flow rate = 3 L/min, and T = 25 °C.

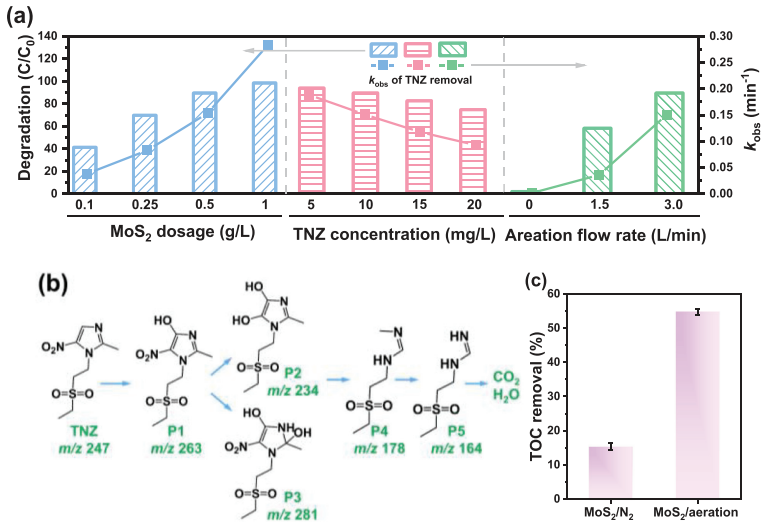

Fig. 3. (a) Effect of operational paraments in MoS_2/aeration system for TNZ degradation. (b) Proposed degradation pathways and (c) TOC removal of TNZ in MoS_2/N_2 and MoS_2/aeration system.

EPR peaks were observed in MoS_2 (Quiescence) system, indicating the aeration is an essential factor for piezo-catalysis. Remarkably, compared with the MoS_2/aeration system, no signal of DMPO-$O_2^{\bullet-}$ could be seen under N_2 atmosphere in the absence of DO, suggesting the generation of $O_2^{\bullet-}$ is from DO in water [35]. In the meanwhile, there was also no TEMPO-$^1O_2$ signal observed in the MoS_2/N_2 system (Fig. 2f), which further confirmed that DO was also crucial in $^1O_2$ formation. Based on these results, it can be assumed that the piezoelectrically polarized e^- reacted with DO to convert into $O_2^{\bullet-}$, then follows the generation of $^1O_2$.

The influence of operation parameters in the MoS_2/aeration system for TNZ degradation was conducted by adjusting MoS_2 dosage (0.1–1 g/L), initial TNZ concentration (5–20 mg/L), and aeration flow rate (0–3 L/min). Fig. 3a shows the degradation efficiencies of TNZ improved with increasing dosage of MoS_2, owing to more active sites available in MoS_2. In addition, the removal rate of TNZ was inversely proportional to the enhancement of initial TNZ concentration, which was because of competitive reactions of ROS by numerous TNZ molecules in such a high-concentration solution. Interestingly, increasing the aeration flow rate allowed MoS_2 to boost TNZ degradation efficiency gradually. It could be believed that drastic water bubbles rupture was able to provide a stronger aeration force with MoS_2 to strengthen the piezoelectric polarization for a higher piezo-potential, thus facilitating a more efficient charges separation for ROS generation. Cycles experiment, TEM, and XRD were carried out to evaluate the stability of MoS_2. From Figs. S7-S9 (Supporting information), the catalytic performance only decreased by 6.1% after four cycles and there was no change in morphology of TEM image and crystallinity. Furthermore, TNZ was treated by the MoS_2/aeration system in different water matrices to assess the effectiveness of MoS_2/aeration system in natural samples (Text S2 and Fig. S10 in Supporting information). The above results imply that MoS_2/aeration system shows a high potential for TNZ degradation in real water.

According to the LC-TOF-MS data (Fig. S11 in Supporting information), five degradation intermediates of TNZ degradation were identified. As shown in Fig. 3b, the procedure of degradation possibly started with the hydroxylation on the *N*-heterocyclic ring to generate **P1**, then **P2** was evolved by further hydroxylation from **P1** [36]. Meanwhile, nitro group of **P1** was also likely to be attacked by hydroxyl group to produce **P3**. Afterwards, the opening of the *N*-heterocyclic ring and the loss of methyl group could eventually lead to **P4** and **P5** [37]. These degradation intermediates were finally mineralized to CO_2 and H_2O, and the TOC removal efficiency of 54.1% was realized, while the MoS_2/aeration system under N_2 atmosphere only exhibited 16.2% of TOC removal, further demonstrating that the presence of DO not only promotes the generation of ROS to facilitate the degradation of TNZ, but also enhances the mineralization rate of TNZ removal (Fig. 3c). Besides, the bioaccumulation factor, developmental toxicity, and mutagenicity of TNZ and its degradation products were analyzed by Toxicity Estimation Software Tool (T.E.S.T). The results and discussion were given in Table S1 and Text S3 (Supporting information).

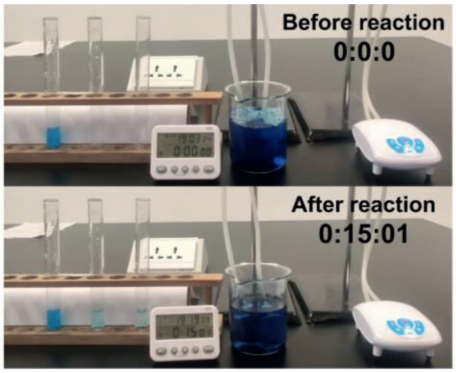

Fig. 4. Screenshots of the video in given times during the piezo-decolorization process of MB. Experimental conditions: [MB] = 10 mg/L, [MoS_2] = 0.5 g/L, aeration flow rate = 3 L/min, and T = 25 °C.

In order to clarify the performance of piezoelectric effect more intuitive, we performed the piezo-decolorization process of methylene blue (MB) and shown in Video S1 (Supporting information) and Fig. 4. Under the turbulence and water bubbles rupture driven by aeration, the color of MB faded from dark blue to light blue in the given time intervals, demonstrating that the aeration-driven piezo-catalysis can be broadly applied in wastewater remediation.

In addition to TNZ, other various antibiotics including ornidazole (ORZ), tinidazole (TNZ), metronidazole (MTZ), secnidazole (SNZ), ciprofloxacin (CIP), sulfamethazine (SMT), sulfamethoxazole (SMX), oxytetracycline (OTC), tetracycline (TC), and doxycycline (DTC) were also used to investigate the piezo-catalytic ability in the MoS_2/aeration system. As shown in Fig. 5, the removal efficiencies reached 93%, 89.5%, 82.1%, 95.2%, 83.1%, 95.1%, 91.6%, 88.1%, 85.2%, and 86.6%, respectively in MoS_2/aeration system, which con-

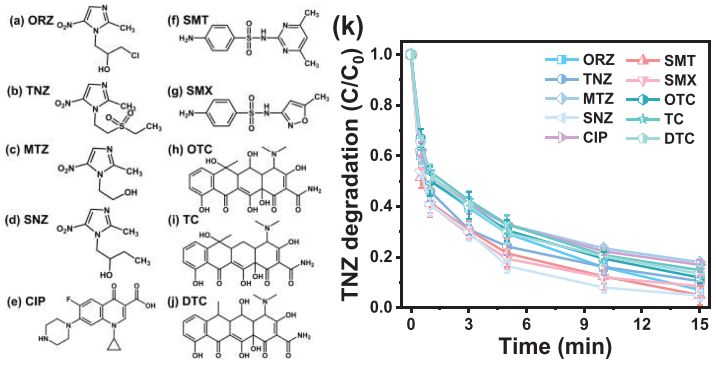

Fig. 5. Structures of the different organic pollutants: (a) ORZ, (b) TNZ, (c) MTZ, (d) SNZ, (e) CIP, (f) SMT, (g) SMX, (h) OTC, (i) TC, (j) DTC. (k) Degradation efficiency of the above ten pollutants in the MoS_2/aeration system. Experimental conditions: [pollutants] = 10 mg/L, [MoS_2] = 0.5 g/L, aeration flow rate = 3 L/min, and T = 25 °C.

vincingly proved that the MoS_2 possesses wide applicability for the elimination of antibiotics under aeration-driven piezo-catalysis in the presence of DO.

Combined with quenching experiments and EPR tests, the reaction mechanism of TNZ degradation in MoS_2/aeration system is proposed as equations (Eqs. 1–7). Under aeration, the piezoelectrically polarized charge carriers (e^- and h^+) are concurrently separated on the surface of MoS_2 (Eq. 1). The piezo-excited e^- reacts with DO to produce $O_2^{\bullet-}$ (Eq. 2), while $HO^\bullet$ is generated by the reaction between remained holes and H_2O (Eq. 3). Then, the holes may oxidize $O_2^{\bullet-}$ to form $^1O_2$ (Eq. 4), and this process is demonstrated by the evident suppression of TNZ removal in the addition of KI (h^+ scavenger) in scavenger experiments (Fig. 2c). Afterwards, the generated $HO^\bullet$ recombined with $O_2^{\bullet-}$ to generate $^1O_2$ (Eq. 5). Moreover, superfluous $O_2^{\bullet-}$ will couple with itself in water to evolve $^1O_2$ (Eq. 6). Finally, $O_2^{\bullet-}$, $HO^\bullet$, and $^1O_2$ are responsible for TNZ degradation (Eq. 7).

$$MoS_2 + \text{vortex} \rightarrow MoS_2\left(e^- + h^+\right) \quad (1)$$

$$e^- + O_2 \rightarrow O_2^{\bullet-} \quad (2)$$

$$h^+ + H_2O \rightarrow HO^\bullet \quad (3)$$

$$O_2^{\bullet-} + h^+ \rightarrow {}^1O_2 \quad (4)$$

$$O_2^{\bullet-} + HO^\bullet \rightarrow {}^1O_2 + HO^- \quad (5)$$

$$2O_2^{\bullet-} + 2H_2O \rightarrow H_2O_2 + 2HO^- + {}^1O_2 \quad (6)$$

$$\text{Pollutants} + O_2^{\bullet-}/HO^\bullet/{}^1O_2 \rightarrow \text{intermediates} \quad (7)$$

In summary, an aeration-driven piezo-catalysis on MoS_2 for TNZ degradation in the presence of DO was investigated. During this piezo-catalytic system, the turbulence driven by aeration not only triggers MoS_2 to generate a piezoelectric potential to drive the transfer of charges, but also provides sufficient DO to produce ROS including $O_2^{\bullet-}$, $HO^\bullet$, and $^1O_2$. Remarkably, DO plays a critical role in generating $O_2^{\bullet-}$ and $^1O_2$ in the piezo-catalytic reaction for attaining high-efficient TNZ degradation and TOC removal within 15 min. Furthermore, the system has great stability and applicability for ten types of antibiotic degradation as well. This work offers a novel way to achieve water pollutant treatment by piezo-catalysis using aeration.

Declaration of competing interest

The authors declare that they have no competing financial interests or personal relationships that could have appeared to influence the work reported in this paper.

Acknowledgments

The study was financially supported by Open Project of State Key Laboratory of Urban Water Resource and Environment, Harbin Institute of Technology (No. ESK202102), the Science and Technology Program of Guangzhou (No. 202201020545), and the Special Fund for Basic Scientific Research Business of Central Public Research Institutes (No. PM-zx703-202204-117).

Supplementary materials

Supplementary material associated with this article can be found, in the online version, at doi:10.1016/j.cclet.2023.108229.

References

[1] B.R. Shah, J. Mraz, Rev. Aquacult. 12 (2020) 925–942.
[2] T. Defoirdt, N. Boon, P. Sorgeloos, W. Verstraete, P. Bossier, Trends Biotechnol. 25 (2007) 472–479.
[3] S. He, Y. Chen, X. Li, L. Zeng, M. Zhu, ACS ES&T Eng. 2 (2022) 527–546.
[4] B.L. Phoon, C.C. Ong, M.S.M. Saheed, et al., J. Hazard. Mater. 400 (2020) 122961.
[5] P. Chaturvedi, P. Shukla, B.S. Giri, et al., Environ. Res. 194 (2021) 110664.
[6] Y. Chen, J. Yang, L. Zeng, M. Zhu, Crit. Rev. Environ. Sci. Technol. 52 (2022) 1401–1448.
[7] B. Ji, S. Fan, Y. Liu, Bioresour. Technol. 350 (2022) 126914.
[8] W.A.W. Mahari, K. Waiho, E. Azwar, et al., Chemosphere 288 (2022) 132559.
[9] T.T. Zhu, Z.X. Su, W.X. Lai, Y.B Zhang, Y.W. Liu, Sci. Total Environ. 776 (2021) 145906.
[10] Z. Liang, C.F. Yan, S. Rtimi, et al., Appl. Catal. B: Environ. 241 (2019) 256–269.
[11] L. Pan, S. Sun, Y. Chen, et al., Adv. Energy Mater. 10 (2020) 2000214.
[12] J. Liu, W. Qi, M. Xu, et al., Angew. Chem. Int. Ed. 62 (2022) e202213927.
[13] M. Zhang, H. Tao, C. Zhai, et al., Appl. Catal. B: Environ. 326 (2023) 122399.
[14] Z. Liu, X. Yu, L. Li, Chin. J. Catal. 41 (2020) 534–549.
[15] J. Wu, W. Chang, Y. Chang, et al., Adv. Mater. 28 (2016) 3718–3725.
[16] J. Hu, C. Yu, C. Li, et al., Nano Energy 101 (2022) 107583.
[17] B. Huo, F. Meng, J. Yang, et al., Chem. Eng. J. 436 (2022) 135173.
[18] S. Lan, C. Yu, E. Wu, M. Zhu, D.D. Dionysiou, ACS ES&T Eng. 2 (2021) 101–109.
[19] S. Lan, B. Jing, C. Yu, et al., Small 18 (2022) 2105279.
[20] S. Lan, X. Ke, Z. Li, et al., ACS ES&T Water 2 (2022) 367–375.
[21] Y. Wen, J. Chen, X. Gao, et al., Nano Energy 101 (2022) 107614.
[22] C.E. Boyd, E.L. Torrans, C.S. Tucker, J. World Aquacult. Soc. 49 (2018) 7–70.
[23] P. Yongphet, R. Ramaraj, N. Whangchai, et al., Aquacult. Eng. 91 (2020) 102119.
[24] S. Sohani, B. Ara, H. Khan, et al., Environ. Res. 215 (2022) 114262.
[25] K. Alagumalai, R. Shanmugam, S.M. Chen, et al., Process Saf. Environ. 148 (2021) 992–1005.
[26] Y. Chen, S. Lan, M. Zhu, Chin. Chem. Lett. 32 (2021) 2052–2056.
[27] W. Ma, B. Yao, W. Zhang, et al., Environ. Sci. 5 (2018) 2876–2887 Nano.
[28] M. Du, Q. Yi, J. Ji, et al., Chin. Chem. Lett. 31 (2020) 2803–2808.
[29] G.C. Lee, L.M. Lyu, K.Y. Hsiao, et al., Nano Energy 93 (2022) 106867.
[30] S. Liu, B. Jing, C. Nie, et al., Environ. Sci.: Nano 8 (2021) 784–794.

[31] J. Wu, Y.G. Sun, W.E. Chang, et al., Nano Energy 46 (2018) 372–382.
[32] X. Zhao, Y. Lei, P. Fang, et al., Nano Energy 66 (2019) 104168.
[33] Q. Si, W. Guo, H. Wang, et al., Appl. Catal. B: Environ. 299 (2021) 120694.
[34] N. Li, M. Shi, Y. Xin, et al., J. Environ. Chem. Eng. 10 (2022) 107420.
[35] X. Li, S. Huang, H. Xu, et al., Chin. Chem. Lett. 33 (2022) 1321–1324.
[36] Y. Zhou, Y. Wu, Y. Lei, et al., Environ. Sci. Technol. 55 (2021) 14844–14853.
[37] A. Acosta-Rangel, M. Sánchez-Polo, A. Polo, et al., Chem. Eng. J. 344 (2018) 21–33.